IAC-18,A6,9,10,x43640

Comparison of New Methods for the Correlation of Short Radar Tracklets

Benedikt Reihs[1,*], Alessandro Vananti[1], and Thomas Schildknecht[1]

[1]Astronomical Institute University of Bern (AIUB), Sidlerstrasse 5, 3012 Bern, Switzerland
[*]Corresponding Author: benedikt.reihs@aiub.unibe.ch

Abstract

Due to the increasing amount of objects in space and the improving sensitivity of modern radar systems, which enable the detection of smaller objects, the number of tracked objects steadily increases together with the load on these systems. This may lead to shorter tracking times of single objects to be able to track as many objects as possible. Such short tracklets have the disadvantage that they may not provide enough information to compute a reliable initial orbit, if they cannot be matched with a known orbit from a catalogue. Instead it becomes necessary to combine multiple short tracklets, which belong to the same object. The identification of these combinations, called correlation, using short-arc radar measurements is the focus of this paper. Based on the concept of attributables, different methods for initial orbit determination and tracklet correlation are developed, which use different combinations of observables. Simulated radar measurements of surveillance campaigns for different orbit types are used to evaluate the functionality of the methods. The results show that it is critical to consider the J_2-gravitational perturbations by the Earth oblateness to achieve satisfactory results. While all methods perform the task successfully, one method based on the classical Lambert problem achieves the best results also with regard to computational performance. Thus, this method is selected for further development and investigation in the future.

Keywords: space debris, radar, correlation, initial orbit determination

1 Introduction

The growing number of objects in space, many of them non-manoeuvrable, pose an increasing risk to the operations of active satellites. A vital component for the mitigation of that risk is the detection and orbit determination of uncontrolled space objects. For objects in Low Earth Orbit (LEO), this task is mainly achieved by radar systems. As radar systems are becoming more sensitive, it is possible to detect smaller and thus also more objects. When an objects passes a radar station, the measurements form a so-called tracklet. In many cases, such a tracklet can already be associated with a catalogued object, in which case it does not pose any additional challenge. If it cannot be matched with a catalogued object, it has to be assumed that this object is a new detection and sufficient data is necessary to estimate an initial orbit.

To get a reliable orbit, it is necessary to combine mutiple tracklets. The challenge of this approach is to identify two or more tracklets which belong to the same object. Such an association is referred to as a correlation in the following. As radar measurements provide positions of the detected objects, it is possible to attempt an orbit determination with the data from a single tracklet and perform the correlation based on the resulting orbits. Such approaches have already been described and evaluated [1, 2]. However, these methods can be expected to become less reliable as the measured tracklets become shorter and thus provide less information and coverage of the orbit.

For short-arc radar tracklets, it was decided to adopt a technique using attributables, which are often applied to optical measurements [3]. To use an attributable, the measured data are fitted as a function over time and one value of this function is used as a single measurement in an attempt to average out the noise and condense the information of the tracklet in a single point. This tech-

nique has already been successfully applied to the correlation of short-arc optical measurements [4, 5]. Concerning radar data, the use of attributables for the correlation and initial orbit determination has already been shown [6] and will be further extended in this work. The goal of this work is to test different combinations of observables from the attributable for the initial orbit determination and test their suitability for the correlation problem.

2 Developed Methods

For the development of the methods, it is assumed that the radar provides four observables, i.e. the range ρ, the range-rate $\dot{\rho}$, the azimuth angle α and the elevation angle δ. With this information the attributable $\mathscr{A}$ can be calculated for each tracklet together with its time t:

$$\mathscr{A} = \{t, \rho, \dot{\rho}, \alpha, \delta\} \; . \tag{1}$$

Additionally, for each observable its uncertainty can be estimated from the residuals of the fit.

Combining two attributables $\mathscr{A}_1$ and $\mathscr{A}_2$ gives a total of eight observables. They are split in two groups, with one group being used for the orbit determination and the other one as the discriminator, i.e. comparing the measured values against the computed values from the calculated orbit to check for matching attributables. Ideally, if the two attributables belong to the same object the difference between the elements in the discriminator should be small. The exact loss function for the correlation decision is given in Section 2.4.

Three different combinations and methods have been developed and other combinations of observables have not been found to allow an estimate of the initial orbit. All methods use pure Keplerian propagation to calculate the initial orbits.

2.1 Method 1: Boundary Positions

$$\begin{array}{rcc} \{\rho_1, \alpha_1, \delta_1, \rho_2, \alpha_2, \delta_2\} & \rightarrow & \text{Orbit} \\ \{\dot{\rho}_1, \dot{\rho}_2\} & \rightarrow & \text{Discriminator} \end{array}$$

Using ranges and angles gives two positions on the orbit and thus yields the classical Lambert problem. Various solutions have been developed for this problem, e.g. recently [7]. Here, we use a variation of the iteration on the semi-latus rectum p (p-iteration [8]) by deriving the orbital elements from the two positions together with the time and the angle between them. The two range-rates remain as the discriminators.

In general, there are several solutions of this problem for different numbers of revolutions and prograde or retrograde orbits, which are all considered in the implementation. From all these possible solutions, the one with the smallest loss function is chosen.

2.2 Method 2: Initial Position and Velocity

$$\begin{array}{rcc} \{\rho_1, \dot{\rho}_1, \alpha_1, \delta_1, (\rho_2, \alpha_2, \delta_2)\} & \rightarrow & \text{Orbit} \\ \{\rho_2, \dot{\rho}_2, \alpha_2, \delta_2\} & \rightarrow & \text{Discriminator} \end{array}$$

For the second method, the range-rate of the first tracklet is included in the orbit generation. The iteration is performed on one component of the velocity vector at time t_1. Together with the range-rate and the orbital plane, the full velocity vector can be derived via the geometry of range-rate and line-of-sight. The orbital plane is calculated by using the second position, although the exact position is not enforced as this would overconstrain the problem. Thus it is possible to use all of the second tracklet's observables in the discriminator as the orbit does not necessarily include the second position. Also for this method, there are multiple solutions for different numbers of revolutions and prograde or retrograde orbits.

2.3 Method 3: Velocity-based Integrals of Motion

$$\begin{array}{rcc} \{\rho_1, \dot{\rho}_1, \alpha_1, \delta_1, \rho_2, \dot{\rho}_2, \alpha_2, \delta_2\} & \rightarrow & \text{Orbit} \\ \{\Delta\omega, \Delta\varphi\} & \rightarrow & \text{Discriminator} \end{array}$$

For the third method, the range-rate of the second measurement is added to the orbit calculation. In this case the iteration parameter is the norm of the first velocity vector, from which its components can be calculated via the orbital plane and the range-rate. The same is true for the second tracklet, for which the norm of the velocity vector is calculated via the vis-viva-equation. A solution is obtained when the combinations of position/velocity have the same angular momentum and orbital energy at both epochs. Such a solution was first proposed in 1977 [9].

Usually it is not possible to connect both points with the same orbit fulfilling the conditions on the range-rate, thus the discriminator is the difference between the orbits, namely the argument of perigee ω and the true anomaly φ. The other orbital elements are the same due to the conditions on the integrals of motion. A similar approach for a discriminator is also found in [10]. With this approach there is only one solution for each prograde or retrograde orbit and there is no additional comparison between different numbers of revolutions.

2.4 Loss Function

To consider also the uncertainty of the measurements, the Mahalanobis Distance is used as the loss function [11]:

$$M_d = \sqrt{\vec{D}_d^T \cdot C_{M,O}^{-1} \cdot \vec{D}_d} \; , \tag{2}$$

with the vector $\vec{D}_d$ as the difference between the observed discriminator and the ones computed from the calculated orbit. The covariance matrix $C_{M,O}$ is the sum of the measurement uncertainties of the discriminators and the covariance of the discriminators based on the uncertainty of the observables used for the orbit determination. This transformation is obtained via numerical differentiation. In practice, each time the resulting Mahalanobis distance from a pair of tracklets is lower than a given threshold, the two tracklets are assumed to belong to the same object, i.e. are correlated.

3 Results

3.1 Simulations

To test all three methods, different observation campaigns are simulated to create radar tracklets. Noise is added with the assumption of uncorrelated white noise for each observable. The assumed noise at a range of $\rho_N = 750$ km is given in Table 1. If the range is larger than ρ_N, the noise is increasing as a square root function [12].

Table 1: Standard deviation σ of noise at $\rho_N = 750$ km.

Observable	σ
Azimuth, Elevation	0.17°
Range	20 m
Rate	20 $\frac{\text{m}}{\text{s}}$

The only visibility constraints are a maximum range $\rho_{\max} = 2500$ km and a minimum elevation $\delta_{\min} = 5^\circ$. For the correlation experiment, a short tracklet of 10s length at a rate of one point per second is cut randomly out of the full pass. A linear least squares fit is applied to this data to estimate the observables and their uncertainties for the reference epoch in the middle of the short tracklet. For the comparisons, each method uses the same set of attributables.

Two survey campaigns are simulated. The first campaign contains 150 LEO objects and runs for 24 hours. The second campaign consists of 150 objects in Highly Elliptical Orbits (HEO), which have a perigee altitude within the range of the radar system, and lasts seven days to make up for the lower number of revolutions and less visible passes of HEO objects.

Two different types of propagation are used: Keplerian propagation without any perturbations and a full numerical propagation containing atmospheric drag, Earth gravitational perturbations, solar radiation pressure and third body perturbations of sun and moon. For this propagation, the free astrodynamics tool Orekit is used [13]. The resulting number of tracklets for the four different simulations is shown in Table 2.

Table 2: Number of tracklets created during the different simulations.

Propagation	LEO	HEO
Keplerian	739	341
Numerical	740	329

3.2 Time Intervals

The following Figure 1 and Figure 2 show the distributions of time between the tracklets in the described simulations. As one would expect, the number of pairs is steadily decreasing towards the total time of the simulation.

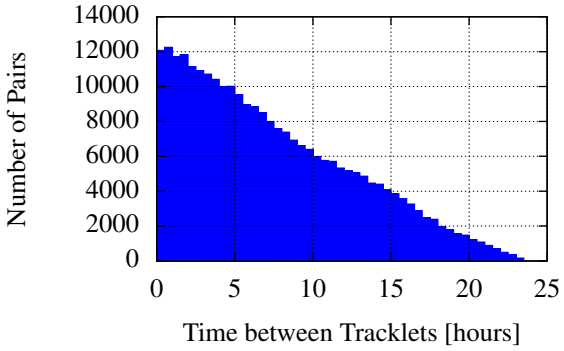

Figure 1: Times between tracklets for LEO case.

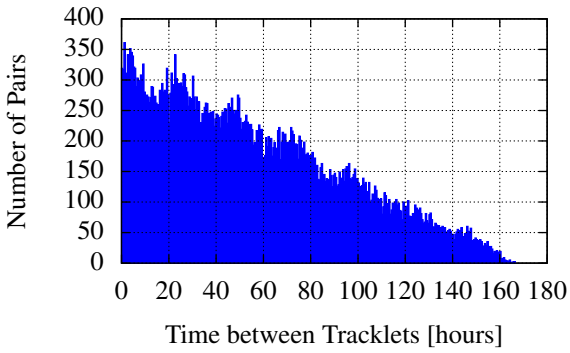

Figure 2: Times between tracklets for HEO case.

3.3 Keplerian Propagation

The idealised case of the two-body Keplerian propagation serves as a basic proof of concept. As all correlation methods use Keplerian propagation internally, the only challenge in this scenario is the noise of the measurements combined with the fitting of the attributables.

This section and the following ones use the terms *true positive* for a correlation between two tracklets

from the same object, *false positive* for a correlation of two tracklets from different objects and *false negative* for no correlation between two tracklets from the same object.

The results for all methods and orbits are shown in Figure 4. All methods reach an acceptable performance with a clearly visible peak of true positive correlations for Mahalanobis distances smaller than 3. For the HEO case, in addition to the false positives, there is also a significant number of true correlations with a wrong orbit in terms of the number of revolutions, i.e. a large offset in the semi-major axis. To sum up this experiment, it is clearly visible that all methods are in principle suitable for the correlation task and the use of attributables is appropriate.

3.4 Numerical Propagation

The simulated measurements based on numerical propagation are used, while the rest of the setup remains exactly the same as in the previous experiment. As shown in Figure 5, the degradation of the results is very strong and none of the methods is working properly. Clearly, no useful correlation can be obtained this way. The few true positives with low Mahalanobis distances belong to pairs of objects which are relatively close together in time. This will be discussed further in Section 3.7.

3.5 Including the J_2 Correction

For satellites in LEO, apart from drag, the gravitational perturbations due to the Earth oblateness, described by the J_2-term in the spherical harmonics of the Earth gravitational field, is the main disturbing force [14]. Its main effects are the rotation of the orbital plane, changing the Right Ascension of the Ascending Node (RAAN, Ω), and the rotation of the Argument of Perigee (AoP, ω). Both can be estimated with analytical formulae based on the orbit's semi-major axis a, eccentricity e and the inclination i with a value of $J_2 = 1.08263 \cdot 10^{-3}$ [15]:

$$\Delta\Omega = -2.06474 \cdot 10^{14} \cdot \frac{\cos(i)}{a^{3.5} \cdot (1-e^2)^2} , \quad (3)$$

$$\Delta\omega = 1.03237 \cdot 10^{14} \cdot \frac{4 - 5\sin^2(i)}{a^{3.5} \cdot (1-e^2)^2} , \quad (4)$$

both in $\left[\frac{\text{deg}}{\text{day}}\right]$ using a in km.

To consider these effects the position at the time of the second measurement is adjusted by two rotations, a comparable approach can be found in [16]. Firstly, the position is rotated around the Earth z-Axis by $(-\Delta\Omega)$ with the standard cartesian rotation matrix $\underline{R}_z$:

$$\vec{R}_2' = \underline{R}_z(-\Delta\Omega) \cdot \vec{R}_2. \quad (5)$$

This operation changes the orbital plane, i.e. both the inclination and the RAAN. Additionally, the angle between the two positions is reduced by $\Delta\omega$, which is effectively the same as a rotation of $\vec{R}_2$ around the orbit normal.

Within the algorithms, the initial orbit is calculated without any corrections and afterwards the corrections are applied in an iterative process until the orbital plane and the Mahalanobis distance have converged, which means that the calculated orbit yields the same corrections as have been applied to calculate it. It should be noted that the internal propagation within the correlators is still pure Keplerian.

The results of the correlation, shown in Figure 6 using exactly the same attributables as in the previous section, are now vastly improved. The quality of the result is nearly as good as the ones shown for Keplerian propagation in Section 3.3.

Additionally, Figure 7 shows the development of true positives, false positives and false negatives over the correlation threshold value of the Mahalanobis distance. The additional vertical lines locate the thresholds, at which 90% of true positives is reached, the increase in false positives is higher than in true positives and the middle between these two points. The closer these lines lie together, the better is the consistency of the results. It can be seen, that a threshold of $M_d = 3$, which was already added to the previous figures, is a good estimate of a threshold for all methods with LEO observations and for method 1 even with HEO objects.

3.6 Example: J_2 Correction

This section gives an example of the effect of the J_2 correction. Figure 3 shows the Mahalanobis distance before and after the J_2 correction for one specific example of the LEO experiment obtained with method 1. Two observations can be made from this plot. Firstly, even without correction a low Mahalanobis distance would indicate a true correlation but for the wrong number of revolutions and thus a large error in semi-major axis. Secondly, the function of the corrected Mahalanobis distance is approximately linear over the number of revolutions towards the minimum. This could allow another layer of optimisation by searching for the correct number of revolutions instead of testing all solutions. Especially in case of a very long time between two tracklets, this could increase the efficiency significantly.

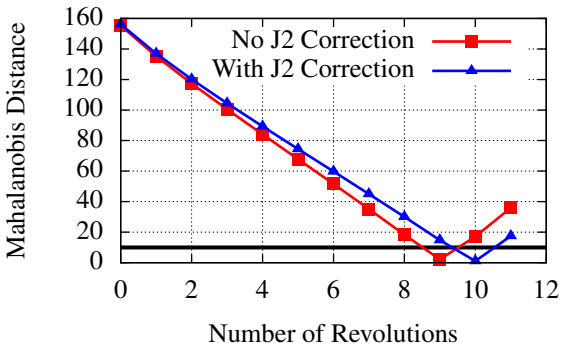

Figure 3: Example of result with and without J_2 correction for a pair of LEO tracklets with method 1.

3.7 Discussion

The presented results have shown that in principle all three methods are able to perform the correlation task successfully with data from a numerical propagation under the consideration of the J_2 perturbation. Analysing the results in detail, method 1 shows the best consistency across LEO and HEO campaigns for the Mahalanobis distance used as a threshold value. Additionally, this is also the fastest method computationally. The other two methods mainly suffer from their use of the velocity vector, which forces various vector calculations in each step of the iteration. For the computational efficiency, it is also very advantageous to be able to use Keplerian propagation. Thus the applied correction iteration allows to avoid the use of numerical propagation, which would slow down the overall process significantly. Concerning the J_2 correction, method 2 also has the problem that it may not be possible to find an initial solution, which matches both the orbital plane, which is wrong due to the perturbations, and the range-rate. This problem also reduces the maximum time between two tracklets or a solution via an estimated correction before the first solution would be necessary.

The effect of the J_2 correction can also be shown with regard to the number of revolutions between two correlated tracklets. Figure 8 shows the number of revolutions for true positives of method 1 for all previously shown scenarios. It can be seen that without the correction, the maximum number of revolutions with a significant number of correlations is approximately 5 for LEO and 8 for HEO. When the corrections are applied, there are also correlations for larger numbers of revolutions comparable to the case with Keplerian propagation.

The large number of correct correlations with a wrong orbit for the HEO campaign is probably due to the repeated measurements at the perigee, which lead to a much smaller coverage of the orbit. Additionally, the HEO attributables have larger ranges than the LEO ones on average, thus also a higher noise level and larger uncertainties.

4 Conclusion

This work has introduced and tested three different methods for initial orbit determination with regard to the correlation of radar measurements. It could be shown that all methods are working and yield acceptable results. Especially, the importance of the J_2 correction has become clear in the process of this work. Combining everything which was learned during the tests of the methods, it was decided that method 1 is the most promising due to its consistency of the threshold value and computational performance. This method will be further extended and tested in the future.

Acknowledgements

The author is supported by the European Space Agency through the Networking/Partnering Initiative.

References

[1] K. Hill, C. Sabol, K. T. Alfriend, Comparison of covariance based track association approaches using simulated radar data, The Journal of the Astronautical Sciences, 59 (2012) 281–300.

[2] A. Vananti, T. Schildknecht, J. Siminski, B. Jilete, T. Flohrer, Tracklet-tracklet correlation method for radar and angle observations, 7th European Conference on Space Debris, Darmstadt, Germany, April 2017.

[3] A. Milani, Theory of orbit determination, Cambridge University Press, Cambridge, UK New York, 2010.

[4] J. A. Siminski, O. Montenbruck, H. Fiedler, T. Schildknecht, Short-arc tracklet association for geostationary objects, Advances in space research, 53 (2014) 1184–1194.

[5] K. Fujimoto, D. J. Scheeres, J. Herzog, T. Schildknecht, Association of optical tracklets from a geosynchronous belt survey via the direct Bayesian admissible region approach, Advances in space research, 53 (2014) 295–308.

[6] G. F. Gronchi, L. Dimare, D Bracali Cioci, H. Ma, On the computation of preliminary orbits for Earth satellites with radar observations, Monthly Notices of the Royal Astronomical Society, 451 (2015) 1883–1891.

[7] D. Izzo, Revisiting Lambert's problem, Celestial Mechanics and Dynamical Astronomy, 121 (2015) 1–15.

[8] P. Escobal, Methods of orbit determination, R.E. Krieger Pub. Co, Huntington, N.Y, 1976.

[9] L. Taff, D. Hall, The use of angles and angular rates, Celestial mechanics, 16 (1977) 481–488.

[10] G. F. Gronchi, L. Dimare, A. Milani, Orbit determination with the two-body integrals, Celestial Mechanics and Dynamical Astronomy, 107 (2010) 299–318.

[11] P. Mahalanobis, On the generalised distance in statistics, Proceedings of the National Institute of Science of India, 2 (1936) 49–55.

[12] M. Skolnik, Introduction to radar systems, McGraw Hill, Boston, 2001.

[13] Orekit, A space dynamics library, 2018, `https://www.orekit.org/`.

[14] N. K. Pavlis, S. A. Holmes, S. C. Kenyon, J. K. Factor, The development and evaluation of the Earth Gravitational Model 2008 (EGM2008), Journal of Geophysical Research: Solid Earth (1978–2012), 117 (2012).

[15] D. Vallado, Fundamentals of astrodynamics and applications, Microcosm Press, Hawthorne, CA, 2013.

[16] H. Ma, G. F. Gronchi, D. Bracali Cioci, Preliminary orbits with line-of-sight correction for LEO satellites observed with radar, ArXiv e-prints (2017), arXiv: `1703.08519 [physics.space-ph]`.

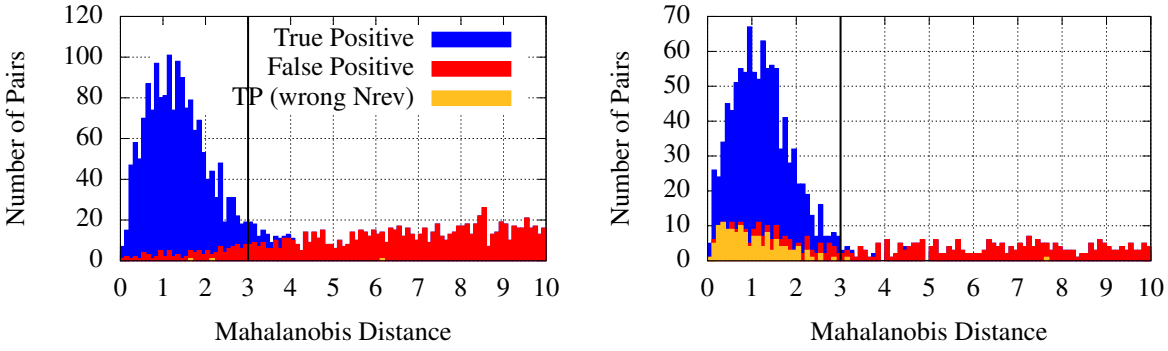

(a) Method 1

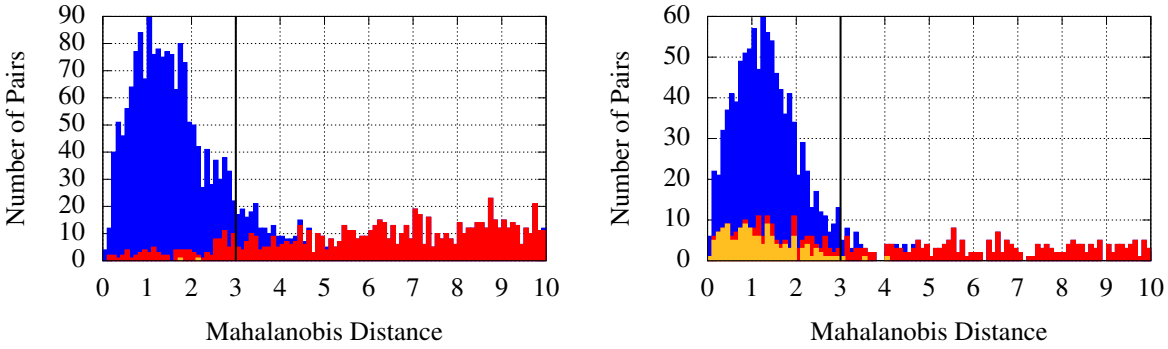

(b) Method 2

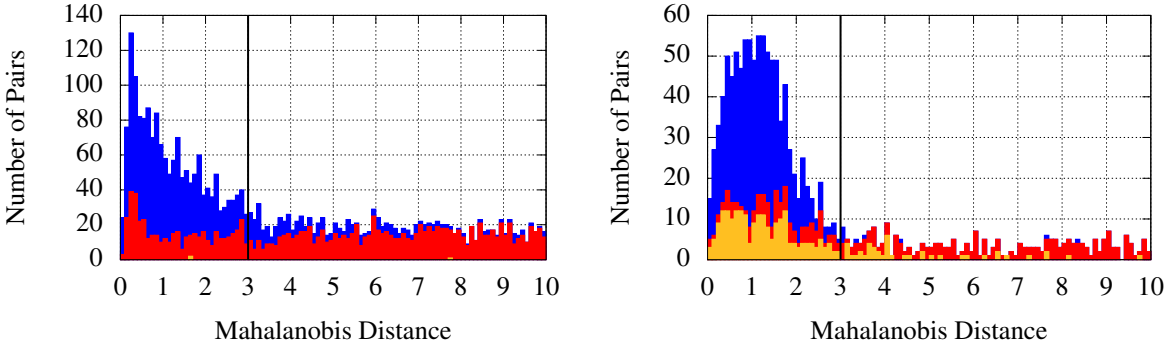

(c) Method 3

Figure 4: Distribution of Mahalanobis distances for Keplerian propagation (Left: LEO, Right: HEO).

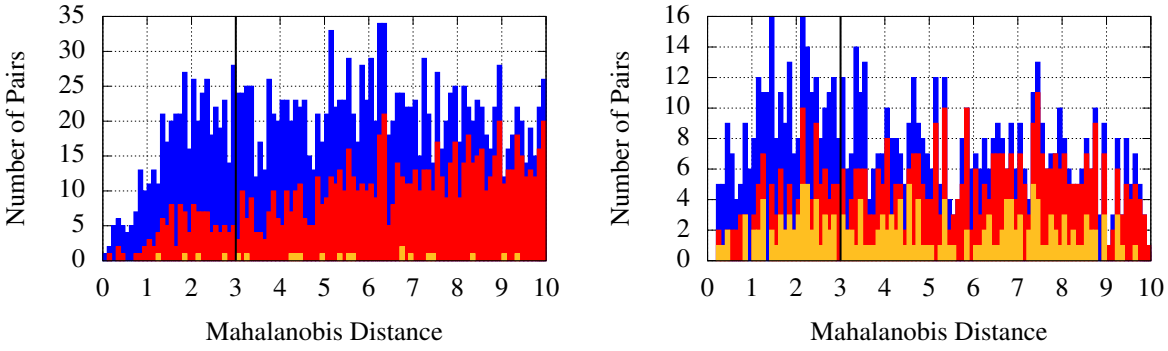

(a) Method 1

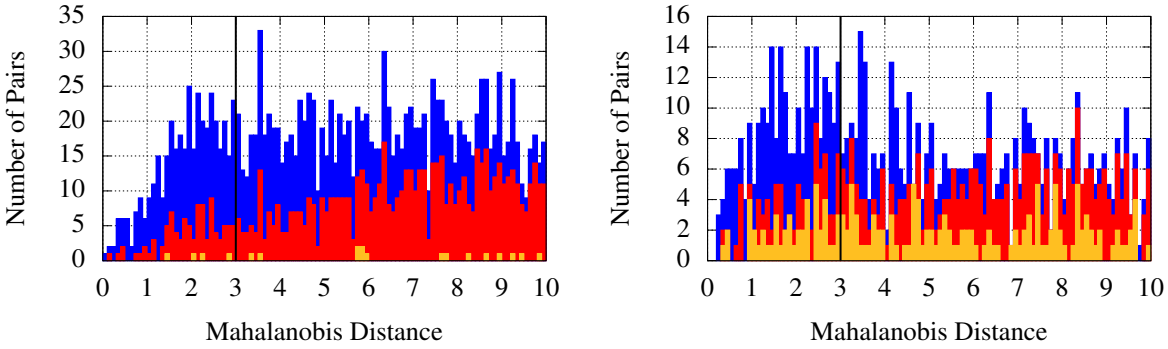

(b) Method 2

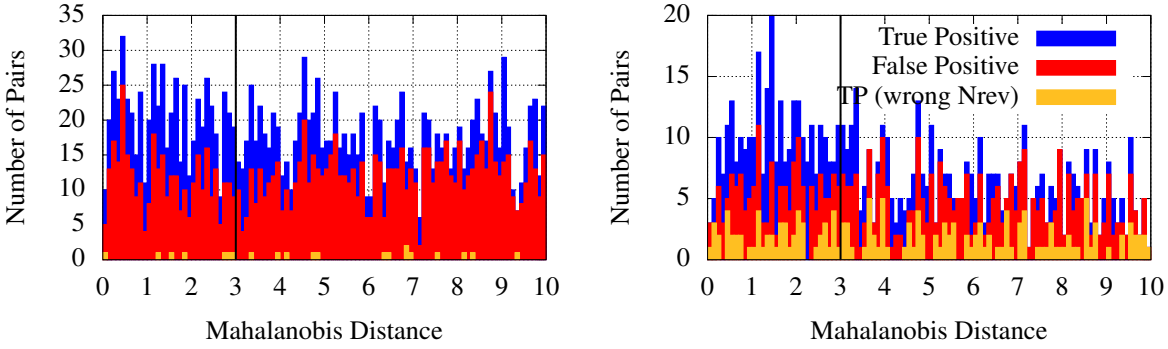

(c) Method 3

Figure 5: Distribution of Mahalanobis distances for numerical propagation (Left: LEO, Right: HEO).

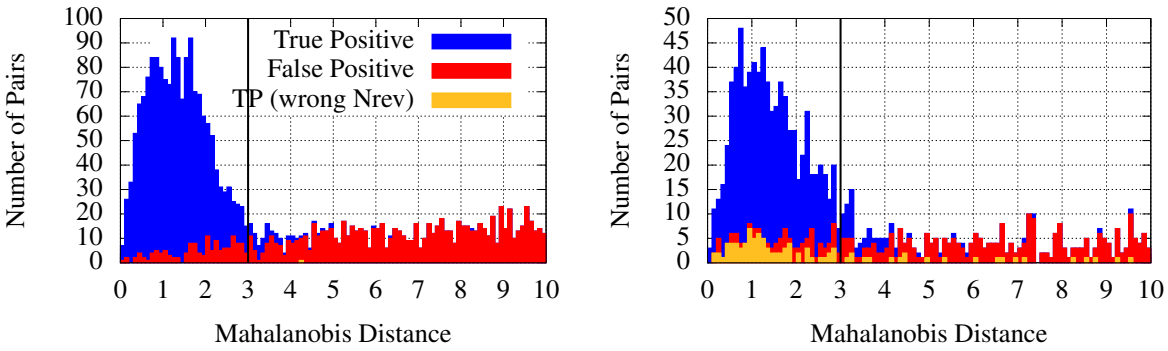

(a) Method 1

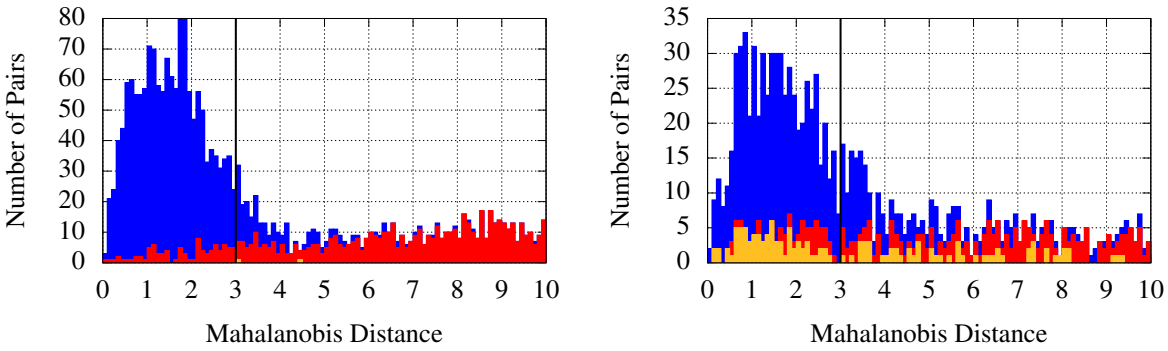

(b) Method 2

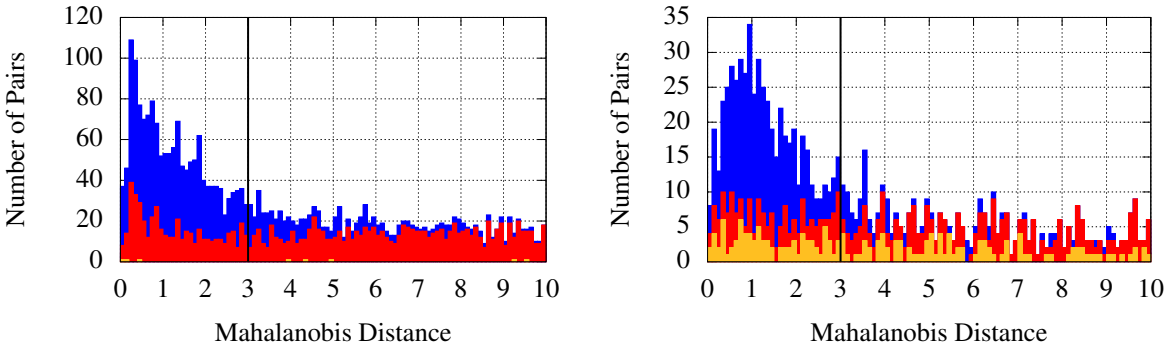

(c) Method 3

Figure 6: Distribution of Mahalanobis distances for numerical propagation with J_2 correction (Left: LEO, Right: HEO).

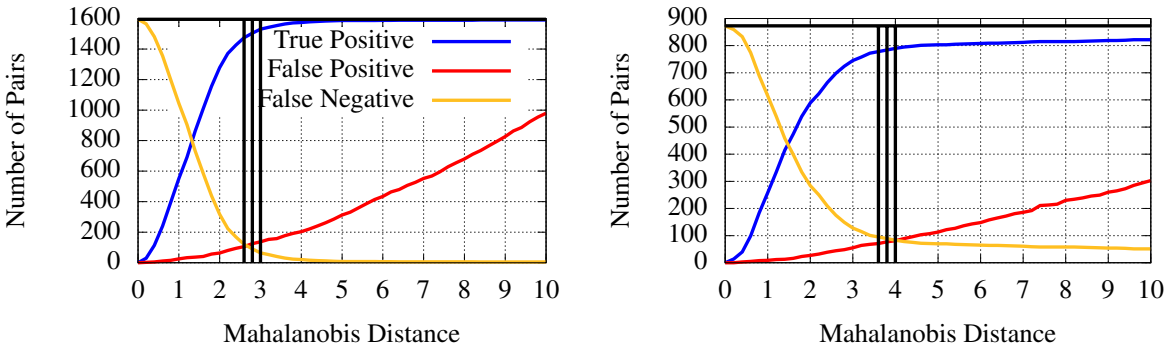

(a) Method 1

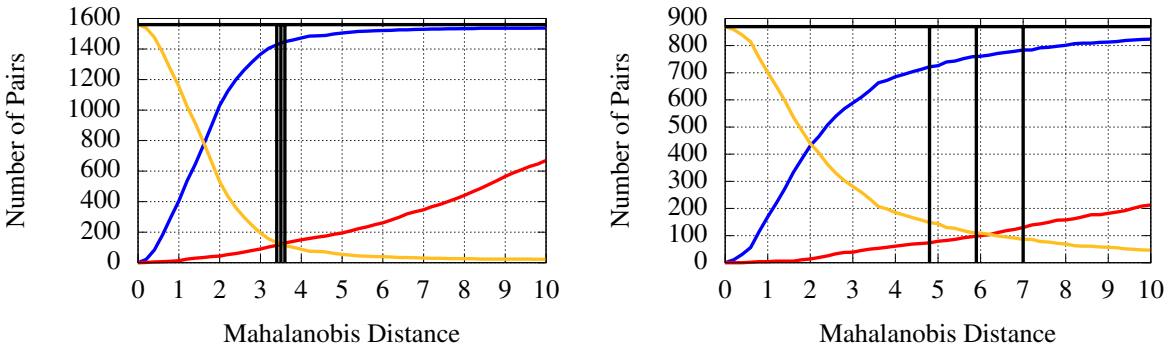

(b) Method 2

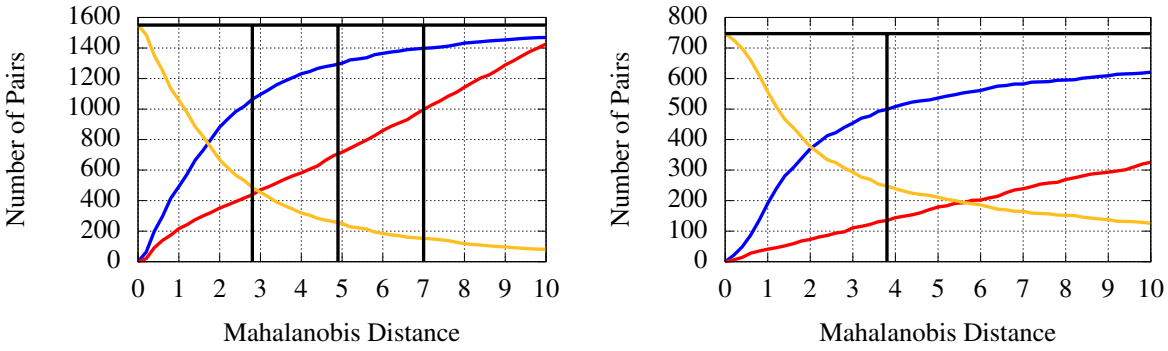

(c) Method 3

Figure 7: Evolution of correlation output over Mahalanobis distances for numerical propagation with J_2 correction (Left: LEO, Right: HEO).

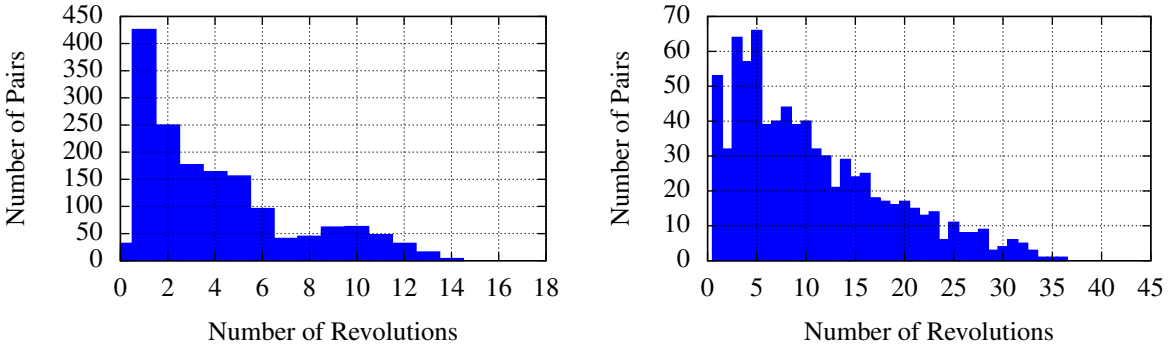

(a) Keplerian propagation

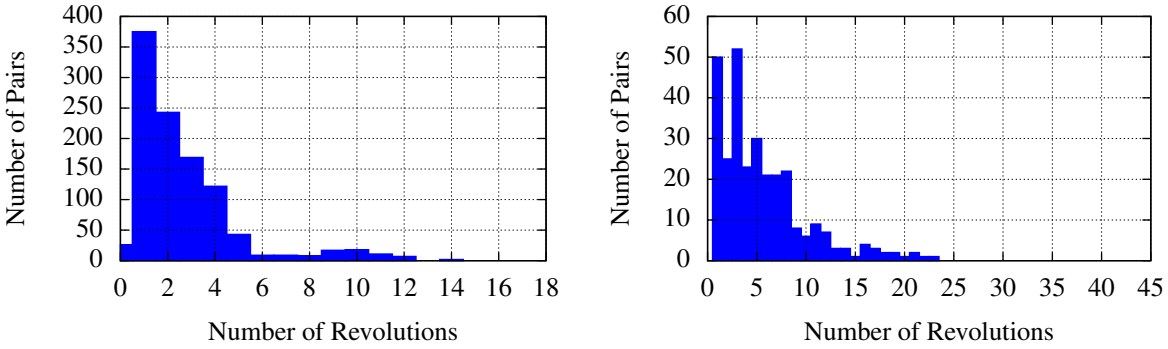

(b) Numerical propagation

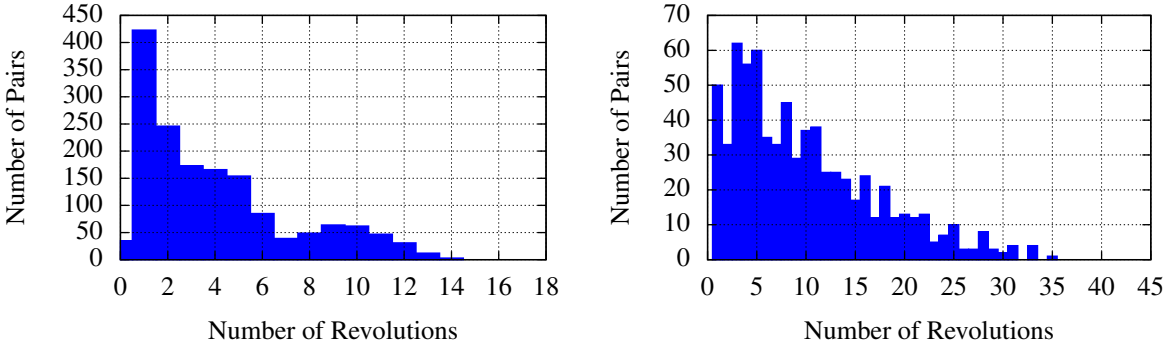

(c) Numerical propagation with J_2 correction

Figure 8: Number of revolutions for true positive correlations using method 1 (Left: LEO, Right: HEO).